PCF-multimode/endless fiber sensor for respiratory rate monitoring

Haneen D. Abdulkareem[1], Ali A. Alwahib[1]*, and Bushara R. Mahdi[2]

1. Laser and Optoelectronics Department, University of Technology-Iraq, Baghdad, Iraq

2. Department of Physics, College of Science, University of Baghdad, Baghdad, Iraq

(Received 28 June 2022; Revised 19 October 2022)

A respiratory monitoring system was proposed based on optical fiber. The sensor consists of photonic crystal fiber (PCF) spliced with multimode fiber (MMF) to fabricate Michelson interferometer. The sensor is inserted into an oxygen mask tube and then put on the nose and mouth to monitor the respiratory rate (*RR*) for different cases. The results showed that when breathing increased, the intensity of light decreased. The intensity of light in the sleeping case of breathing was more intense than that when the intensity of working sport was measured. The working sport case was a higher transmittance than that of sleeping. The sensitivity of the sensor was also measured to be 231.9 pm/RH.

Document code: A **Article ID:** 1673-1905(2023)01-0008-6

DOI https://doi.org/10.1007/s11801-023-2114-1

Breath could be a preparation of oxygen entering the lungs and coming to the body's cells, as well as the forms that cause carbon dioxide out of the body through the nose and mouth[1,2]. Healthcare monitoring is of prime significance due to the instantaneous information provided for physical health[3-5]. Respiratory significance and gas trade can be identified by utilizing the contrasts in temperature, mugginess, and carbon dioxide (CO_2) of respiratory wind current. Also, it is conceivable to screen respiratory exercises by calculating the varieties in thoracic and stomach circumferences[6]. The drive and control of breaths is an intricate system involving the circulatory, pulmonary, and central nervous systems. Chemoreceptors throughout the body monitor for hypoxia and hypercarbia, altering respiratory rate (*RR*) to maintain organ perfusion and optimal pH. Evidence has shown *RR* to be a better predictor of cardio-pulmonary deterioration than blood pressure and pulse rate[7-9]. Presently, fiber optic sensors are utilized to reveal the distinct body and chemical factors of clinical avails[10]. Those sensors are typically classified as extrinsic sensors, in which the fiber optic acts as an ambiance to move the light including the properties (for example, depth, phase, and frequency) are adjustable through the measured, intrinsic fiber optic sensors, the location of the fiber optic, through his efforts, the detecting specifics[11]. Sensors from this two-dimensional magnificence permit spreading the simple components of fiber optic sensors (e.g., photodetector, light supply) far from the element of the sensing, on the way to creating small-scale sensors and hybrid systems[12].

SHAO et al[13] illustrated a test stickiness sensor based on photonic crystal fiber (PCF) manufactured by sandwiching a decrease between PCF and a standard single-mode fiber. The decrease and collapsed locale in PCF energize high-order modes and couple them with center mode to create a Michelson interferometer. MA et al[14] designed a breathing detecting framework utilizing PCF sort LMA-10, outlined for unending single-mode fiber. The interferometer was fabricated by splicing PCF with single-mode fiber, but the PCF segment was ensured with a glass tube protected with another metallic tube. This research proposed a highly respiratory-sensitive sensor based on PCF combined with multimode fiber (MMF) on one side that provides a Michelson interferometer by using a laser as a source in the visible spectrum.

The sensor structure is based on Michelson interferometer. The fabrication of the interferometer includes cleaving and fusion splicing, which can be conducted with standard fiber tools and equipment. The conventional multimode and PCF (LMA-10) were applied. LMA-10 optical fiber has a six-fold symmetry. The core and outer diameters are 10±0.5 μm and 125±2 μm, respectively. The diameter of the voids is 3.1 μm, and the separation between the consecutive voids (pitch) is 6.6 μm. The effective refractive index difference between the core and a dominant high-order mode allows for the phase difference when the implicated mode spreads in the PCF[14]. A short section of PCF length of 3.5 cm was used in this sensor. Firstly, the PCF's striper was used to take off the shielding to prepare the fiber for fusion splicing, and the coating was then stripped using standard fiber stripping techniques,

* E-mail: Ali.A.Alwahib@uotechnology.edu.iq

such as the JIC-375 tri-hole fiber with a 125 μm cladding of whether the succeeding splice is a mechanical or fusion splice, and cleaving an optical fiber is one of the processes in preparing for a fiber splice operation. Splicing with normal MMF using a mechanical fusion splicer is the last step (MFS-60S). The PCF is spliced with MMF from one side to fabricate an endless optical fiber sensor, as shown in Fig.1(a). A very few micrometers in the collapsed region of PCF-MMF were tapering by using a conventional fusion splicer to control the tapering by arc time and arc power. The tapering fibers were observed using a microscope that was 350 μm, as shown in Fig.1(b).

The MMF was spliced with LMA-10 PCF to fabricate the designed sensor head, because of taking advantage of all light patterns, and gives a result for any pattern. If we use it as a single mode optical fiber, the patterns passing through it are specific, and their number does not exceed a few.

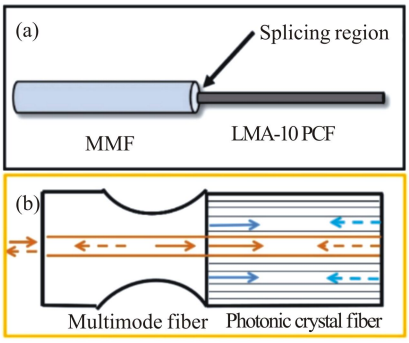

Fig.1 (a) Splicing of MMF-PCF; (b) Tapering region of MMF-PCF

The experimental setup is shown in Fig.2. A 650 nm laser source was connected with the fabrication sensor by the 3-dB fiber optical coupler 50/50. The fiber optical coupler divided the input signal into two parts, namely, one went to the sensor, and the other went to the optical spectrometer (spectrometer-HR2000) when the spectrometer was connected with personal computer (PC) to show the data results[15]. When the signal reaches the sensing surface, this surface will function as a reflected mirror to the signal. The PC is the destination of the reflected signal from the second arm of the optical coupler throughout the spectrometer. The open voids at the end of the PCF make it possible to work the sensor for multi-purposes. However, the response time is slow[14]. The process was repeated for each of the different breathing cases.

The sensor was placed into a thin glass tube to confine moisture inside the sensor and protect it from external influences, as shown in Fig.3(a) and (b). The tube was inserted into the oxygen mask, as shown in Fig.3(c), and connected the sensor to the optical coupler. The oxygen mask was placed and evaluated on the person's face. The inhalation and exhalation were calculated at each breathing process and sensing the moisture associated diameter, then using cleaver Fujikura (CT-30), regardless with the inhalation and exhalation processes.

The Michelson interferometer is a typical optical interferometry setup. A light source is split into two arms using an optical coupler. Each of the light beams is reflected toward the optical coupler, which employs the superposition principle to combine their amplitudes. The resulting interference pattern is usually pointed at a photoelectric detector or camera that is not facing the source. The two light paths of the interferometer can have varying lengths or comprise optical components or even materials that are evaluated for various uses. This sensor was first used on normal air and considered as a reference, and then it was used on daily human activities, such as sitting, walking, jogging, exercising, and sleeping. The light intensity was calculated in each case using an optical spectrometer, and the absorbance and sensitivity were calculated.

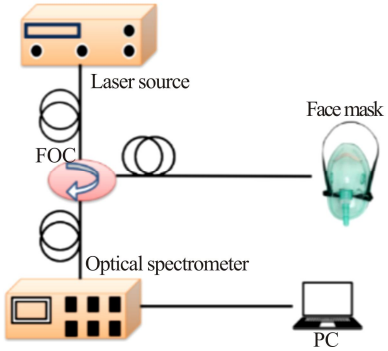

Fig.2 Schematic of sensor setup

Fig.3 Pictures of (a) the sensor, (b) the sensor placed into a thin glass tube, and (c) the tube inserted into the oxygen mask

To simulate the optical fiber sensor, Fig.4 shows the cross-section of the proposed LMA-10 PCF sensor, designed by using COMSOL Multiphysics 5.6 program[16] that consists of a core diameter with 10 μm diameter and air holes arranged in six symmetry with 3.1 μm diameter and distance between them of 6.6 μm and with fused silica cladding with 125 μm. The aqueous analyte layer, with a refractive index n_a, was used to function as the sensing medium. The perfectly matched layer (PML) is a boundary condition that absorbs the scattered electromagnetic waves, helping to improve the numerical analysis. After the design geometry and selected materials ended, define mesh to supply precision of both arrangement and time for calculation to utilize

meth. As a common run of the show, it is a substance with a vast number of triangles. At whatever point, the get the finest.

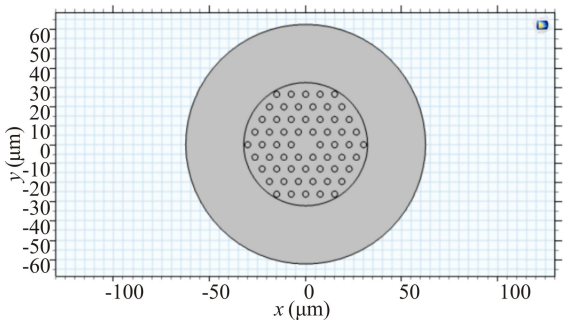

Fig.4 Cross-section of the proposed sensor based on PCF

The sensor was assessed by measuring breathing states. The light intensity was calculated as a function of wavelength. Fig.5 shows the reference wave when the air was used (reference) compared to the intensity at different respiration states. The wavelength range was from 630 nm to 700 nm. The intensity of the laser beam increased gradually from 83.05 as a function of the wavelength at 632.04 nm. When it reached the maximum intensity of 104.56, the wavelength was 655.82 nm because of the red laser source, and then decreased gradually to the reached minimum intensity of 673 nm. As a function of wavelength, the higher the breathing rate, the lower the light intensity. An increase in the breathing rate leads to an increase in the sensor absorption, and thus the resulting intensity decreases.

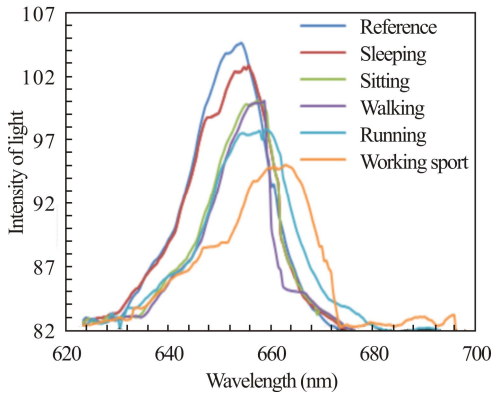

Fig.5 Reflection spectra of the 3.5-cm-long LMA-10 PCF interferometer with different breathing cases

It is obvious from Fig.5 that the resonance wavelength shifted from 657.17 nm to 664.33 nm as the speed of breathing increased. The red shift of the resonance wavelength appears with the increase in speed of breathing, because this sensor senses the humidity content in the exhale. In general, it is assumed that the exhaled breath contains close to 100% of relative humidity. When the *RR* is high and the exhalation occurs, the sensor will mesh was more exact, it would take a longer time for the simulation operation, and after that, the recreation will sense the amount of humidity that would be higher than the amount of humidity associated with slow breathing, and therefore the intensity would decrease.

The intensity in all cases progressively increased until it reached the highest value at the wavelength of the red laser and then went back down. The intensity was 102.8 at 657.17 nm wavelength. Therefore, the highest intensity in the state of sleep is the lowest rate of respiration, approximately 10 breaths per minute. At the normal state of breathing (sitting), the intensity gradually decreased at each state of breathing. In the sitting state, the intensity was 100 at 658.96 nm wavelength. The *RR* increased because the walking state was close to the normal state. However, the intensity was 99.87 at 659.85 nm wavelength, close to the previous state. The *RR* is approximately 14 breaths per minute. In the two last cases, it was less intense because running and working sports increased the *RR*, which is approximately 30 or more, so the intensity of light at running was 97.8 at 660.75 nm wavelength. In contrast, the intensity at working sport, considering the lowest intensity and highest *RR*, was 95.01 at 664.33 nm wavelength. As a result of all cases, red shift wavelength was observed at the higher *RR* and the lower intensity.

In the LMA-10 PCF, the holes have the coefficient of the refractive index of air that is 1, so it is less than the refractive index of the core, and thus the principle of total internal reflection is achieved. But when adding the material, whether air with different parameters or humidity, its concentration is surely variable and therefore its refractive index changes, meaning that the relationship of the refractive index is a direct relationship with the concentration. The greater the change, the greater the sensitivity. The results normally differ according to the case of the tester. If healthy, the results are ideal for different breathing cases, because the *RR* is in normal quantity, while in the case of sickness or respiratory problems, the breathing rate is outside the normal limits, and therefore the results are not ideal.

The principle of the figure of merit (*FOM*) is a significant parameter used to evaluate the performance of the sensors. A large *FOM* indicates high detection accuracy. Additionally, it helps to expand the detection limit. *FOM* can be evaluated as follows

$$FOM\ (\%\ \mathrm{RH}^{-1})=S_{\mathrm{W}}/FWHM, \tag{1}$$

where S_{W} is the wavelength sensitivity and *FWHM* is defined as full-width half maxima. *FOM* was calculated for each case as also shown in Tab.1. The higher value was for walking and the lower value was for sleeping.

Transmittance (*T*) is the fraction of incident light that is transmitted. In other words, it is the amount of light that “successfully” passes through the substance and comes out the other side. Fig.6 shows the transmittance of light as a function of wavelength. So, to calculate transmittance, we used this equation

$$T=I_{out}/I_{in}, \quad (2)$$

where I_{in} is the intensity of incident light, and I_{out} is the intensity of that light after it passes through the sample. Fig.6 shows the opposite results of Fig.5, because the measured intensity was divided by the reference intensity. Therefore, the working sport was the highest transmittance of 0.857 2 at 653.13 nm wavelength. Less transmittance was at sleeping at the value of 0.965 3 at 651.79 nm between the other cases from running to sitting with a value of 0.908 5 at 648.65 nm for running and 0.916 6 at 649.1 nm for sitting, and finally at 0.906 2 at 647.75 nm for walking (Tab.2).

Tab.1 Numerical intensity results of the sensor

Breathing cases	Transmittance	Shifting wavelength (nm)
Working sport	0.857 2	653.13
Running	0.908 5	648.65
Walking	0.906 2	647.75
Sitting	0.916 6	649.10
Sleeping	0.965 3	651.79

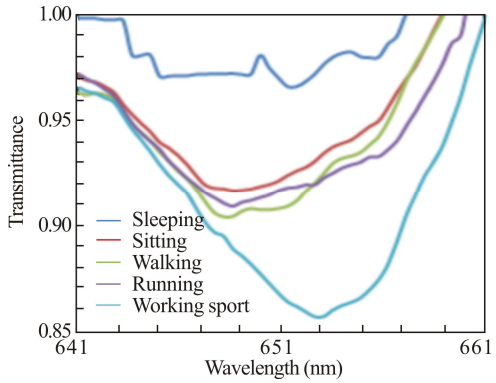

Fig.6 Transmittance spectra of the 3.5-cm-long LMA-10 PCF interferometer with different breathing cases

Tab.2 Numerical transmittance results for the proposed sensor

Breathing cases	Intensity of light	Shifting wavelength (nm)	Figure of merit
Sleeping	102.8	657.17	0.012 0
Sitting	100.0	658.96	0.016 1
Walking	99.87	659.85	0.020 7
Running	97.80	660.75	0.015 2
Working sport	95.01	664.33	0.014 7

The wavelength shift of humidity is ranged between 1—10 nm. The external disturbance will push the signal to shift more than 20 nm. If the effect of the external disturbance is small (the same range of humidity shift), try to separate it. In this experiment, the optical fiber sensor was fixed and protected to prevent an external effect, and this condition is important in any type of optical fiber sensor.

Sensor's sensitivity was calculated by fabricating the breathing sensor based on humidity absorption and calculating the shifting wavelength. The red shift of the resonance wavelength with the increase in speed of breathing because of this sensor senses the humidity content in the exhale. Therefore, the higher the *RR*, the more moisture in the exhale increased, and thus increased the wavelength shifting. So, Fig.7 shows the relationship between shifting wavelength and relative humidity, which is linear. By taking the slope of the curve, we calculated the sensor's sensitivity to be 231.9 pm/%RH. The response time of this sensor was also calculated to be 1.7 s.

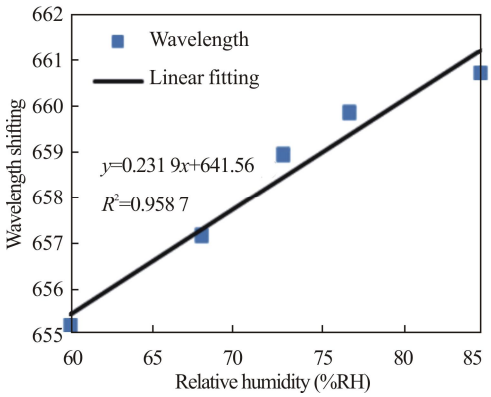

Fig.7 Relation between wavelength and relative humidity for the breathing sensor

Several criteria determine the effectiveness of any sensor. The following are the most important of these criteria.

Resolution: The resolution of an analyte is defined as the capacity to detect even the slightest change in the analyte. It should be noted that the resolution is not a feature of the sensor but instead of the detector itself. The higher the detector's resolution, the higher the sensing probe's resolution. Hence the resolution of a sensing probe is limited to that of the detector.

$$R=\Delta RH/\Delta\lambda*\Delta\lambda_{DR}, \quad (3)$$

where $\Delta RH/\Delta\lambda$ is the (1/sensitivity) of the sensor and $\Delta\lambda_{DR}$ is the spectral resolution of the spectrometer that is 0.05 nm.

Limit of detection (*LOD*): The detection limit in localized surface plasmon resonance (LSPR) sensing is defined as the most minor change in refractive index that can be detected, calculated as follows

$$LOD=R/S, \quad (4)$$

where R is a resolution and S is the sensitivity. Therefore, to improve a sensor's detection limit, one would have to increase the sensor's sensitivity and reduce the resolution. So, these parameters were calculated to the sensor and the resolution was 0.215 RH, and *LOD* was 9.275 pm. The confinement loss was calculated from the following equation

$$L_C=8.686*k_0*\mathrm{Im}(n_{eff}) \ \mathrm{dB/m}, \quad (5)$$

where $\mathrm{Im}(n_{eff})$ denotes the imaginary part of the effective refractive index, and $k_0=2\pi/\lambda$ represents the free space wave number. Fig.8 shows the electric field distributions

for *x* and *y* polarization core modes. These results were obtained at the phase meshing condition and with an analyte refraction index of 1.331, 1.332, 1.333, 1.334, and 1.335 at 650 nm, respectively. The confinement loss spectra for the *x*, *y*, and *x*-*y* polarization were plotted, as shown in Fig.8.

From these results, the values of confinement loss vary from 6.951×10^{-12} dB/m to 4.233×10^{-13} dB/m. For 1.334, it is a higher value, and for 1.332, it varies from 5.959×10^{-12} dB/m to 4.682×10^{-13} dB/m, which is a lower value, and other RI allied between them.

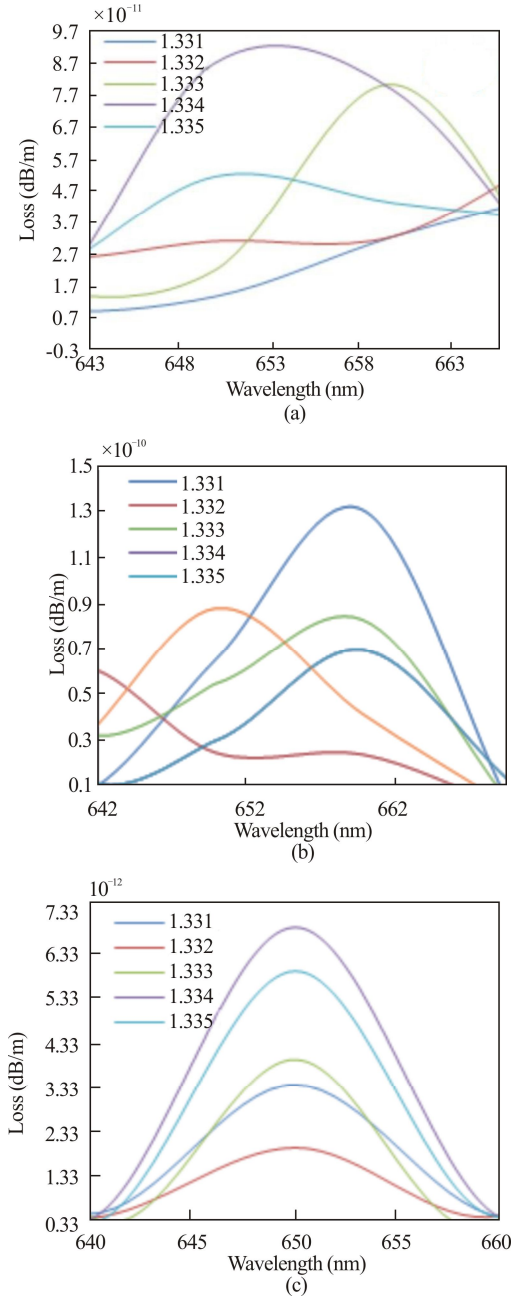

Fig.8 Wavelength-dependent loss spectra for different analyte RIs: (a) *y* polarization; (b) *x* polarization; (c) *x*-*y* polarization

A successful respiratory monitoring system based on an LMA-10 PCF interferometer has been developed. The system monitored *RR*s for various activities based on calculating light intensity. When the *RR* increased, the light intensity decreased and made shifting wavelength for each activity. The highest intensity in the state of sleep is the lowest rate of respiration. In the sitting and walking states, the intensity decreased because the *RR* increased in those cases, and the last states (running and working sports) were less intense. The transmittance of this sensor was also measured.

Statements and Declarations

The authors declare that there are no conflicts of interest related to this article.

References

[1] ARIFIN A, AGUSTINA N, DEWANG S, et al. Polymer optical fiber-based respiratory sensors：various designs and implementations[J]. Journal of sensors, 2019, 2019：7-12.

[2] HALEEM A, AL-OBAIDY A H, HALEEM S. Air quality assessment of some selected hospitals within baghdad city[J]. Engineering and technology journal, 2019, 37(1)： 59-63.

[3] ZHANG X, AI J W, ZOU R P. Compressible and stretchable magnetoelectric sensors based on liquid metals for highly sensitive, self-powered respiratory monitoring[J]. ACS applied materials and interfaces, 2021, 13(13)：15727-15737.

[4] HATAMIE A, ANGIZI A, KUMAR S, et al. Review-textile based chemical and physical sensors for healthcare monitoring[J]. Journal of the electrochemical society, 2020, 167(3)：1-15.

[5] SU K, YANG Y, ZHAO T, et al. A wireless energy transmission enabled wearable active acetone biosensor for non-invasive prediabetes diagnosis[J]. Nano energy, 2020, 74：104941.

[6] BENNETT A. Monitoring of vital bio-signs by multimode speckle based optical fiber sensor[J]. Optics express, 2020, 28(14)：20830-20844.

[7] ROSSOL S L, YANG J K, TONEY-NOLAND C, et al. Non-contact video-based neonatal respiratory monitoring[J]. Children, 2020, 7(10)：171.

[8] DINH J B T, NGUYEN T, PHAN H P, et al. Stretchable respiration sensors：advanced designs and multifunctional platforms for wearable physiological monitoring[J]. Biosensor and bioelectronics, 2021, 166：112460.

[9] HILL S H, ANNESLEY B. Monitoring respiratory rate in adults[J]. British journal of nursing, 2020, 29(1)：1-12.

[10] HASSAN O, AL-AZAWI R, MAHDI B. Image processing technique for zinc ion sensing using a crystalline fiber sensor[J]. Engineering and technology journal, 2021, 39(10)：1539-1543.

[11] HEMALATHA R, REVATHI S. Photonic crystal fiber for sensing application[J]. International journal of

engineering advanced technology, 2020, 9(5)：598178.

[12] MONFARED Y E, AHMADIAN A, DHASARATHAN V. Liquid-filled highly asymmetric photonic crystal fiber Sagnac interferometer temperature sensor[J]. Photonics, 2020, 7(2)：33.

[13] SHAO M, SUN H, LIANG J, et al. In-fiber Michelson interferometer in photonic crystal fiber for humidity measurement[J]. IEEE sensors journal, 2021, 21(2)：1561-1567.

[14] MA J, YU H H, JIANG X, et al. High-performance temperature sensing using a selectively filled solid-core photonic crystal fiber with a central air-bore[J]. Optics express, 2017, 25(8)：9406.

[15] SUHAILIN F H, ALWAHIB A A, KAMIL Y M, et al. Fiber-based surface plasmon resonance sensor for lead ion detection in aqueous solution[J]. Plasmonics, 2020, 15：1369-1376.

[16] FAKHRI M A, ABDULRAZZAQ M J, ALWAHIB A A, et al. Theoretical study of a pure $LiNbO_3$/quartz waveguide coated gold nanorods using supercontinuum laser source[J]. Optical materials, 2020, 109：110363.